Heterogeneous structure in colloidal systems: The role of the microion disposition

Kenneth S. Schmitz
Department of Chemistry, University of Missouri–Kansas City, Kansas City, Missouri 64110
(Received 4 February 2002; revised manuscript received 13 September 2002; published 16 December 2002)

Under certain conditions colloidal systems exhibit a heterogeneous structure sometimes referred to as a ''two state'' structure, ''spinodal instability,'' or a ''phase separation.'' The present study focuses on the ''orbital model'' for the description of two geometries of colloidal clusters: a 7-particle diamond shape array and an 8-particle simple cubic array. The orbital model envisions the distribution of the microions as being dictated by the specific configuration of all the macroions in the system, in much the same way that electron distributions in molecules are determined by the array of atoms. Brownian dynamics simulations were performed as two similar clusters approached each other in rectangular cells at the volume fraction of $\phi_p = 0.01$. The number distributions of both the counterion and coion species were determined three ways: the one-dimensional projection along the long axis of the computations cell; the three-dimensional number distributions in ''real'' space; and a ''constant concentration'' contour profile. It was found that as the two clusters approached each other the diamond cluster system became less stable whereas the simple cubic cluster system became more stable. This difference in behavior is attributed to the relative abilities of these structures to ''share'' counterions and the exclusion of the coions.

DOI: 10.1103/PhysRevE.66.061403 PACS number(s): 82.70.Dd, 64.10.+h, 83.10.Kn

I. INTRODUCTION

The structure of colloidal suspensions and polyelectrolyte solutions is an interesting topic because of the long range electrostatic interplay of the macroions and microions, with the more or less passive involvement of the solvent particles. Recent experimental observations of ''crystalline'' structure (highly ordered distribution of macroions) that coexist with either a ''liquid'' structure (disordered or random distribution of particles) [1–4] or a ''void'' structure (absence of colloidal particles) [5] have added to the mystique of these systems. These ''two-state'' structures are not an artifact of data analysis as these structures can be directly viewed by digital video microscopic (DVM) methods [1–4] and confocal laser scanning microscopy (CLSM) methods [5–8].

The usual approach for characterization of the physical properties of colloidal systems is through the pair potential, which may either be the purely repulsive form of the Derjaguin-Landau-Verwey-Overbeek (DLVO) potential [9] or the repulsive-attractive form of the Sogami-Ise (SI) potential [10]. Within the past few years volume-term (VT) theories have been employed for systems that exhibit a ''phase transition'' [11–13]. The VT models emphasized that colloidal systems cannot be viewed solely in terms of the macroion-macroion pair interactions but must also include the contribution of the microions to the stability of the system. The VT formalism started with the total Helmholtz free energy of the system from which the Gibbs free energy was obtained by standard relationships with the chemical potentials, Helmholtz free energies, and the Gibbs free energies. It was shown, however, that the formalism of the VT approach for the calculation of the chemical potential of all charged species associated with the DLVO pair interaction resulted in a repulsive-attractive Gibbsian form for the pair interaction [14,15].

The VT interpretation of the thermodynamic instability is that the driving force resides in the microions and that the macroions, via their coupling with their counterions, are obliged to follow their neutralizing counterparts and thus forms the ''dense'' region in the suspension. This mechanism is exemplified in Fig. 3 in the paper by Warren [13], where the counterion cloud is described as providing a ''potential well'' for the macroion. This represents, therefore, the weak perturbation limit as likewise present in the DLVO theory. If the ''weak perturbation'' hypothesis is correct then the distribution of the microions should not be significantly altered as two macroions approach each other. On the other hand, if the weak interaction hypothesis is incorrect then there will be substantial alterations in the microion disposition. The present study focuses on the disposition of microions for ''test'' macroion systems in which added electrolyte is present.

II. "ORBITAL" MODEL OF COLLOIDAL CLUSTERS

The basis of our approach is that of Bader and co-workers [16,17] on their description of chemical bonding in molecules. The question addressed in their studies was as follows: Which atoms in a molecule were chemically bonded to each other? The function of interest was the square of the electronic wave function, $\rho_e = \psi^2$. The essence of this view is that vector gradients in the electron density, $\nabla \rho_e$, could determine which specific atoms interacted with each other and which specific atoms engaged in chemical bonding. Atom-atom interactions were said to occur if a ''corridor'' was defined by the vector gradients. Chemical bonding between atoms occurred for closed circles defined by $\mathbf{n} \cdot \nabla \rho_e = 0$, where $\mathbf{n}$ is a normal vector to the closed surface. This method was adapted to colloidal clusters where the potential field set up by the macroions at the position $\mathbf{r}$, $\Psi_M(\mathbf{r})$, functioned in the same way as ρ_e. This method was referred to as the juxtaposition of potential fields (JPF) method [18–20].

A condition of equilibrium in the solution part of the colloidal system is that the chemical potential everywhere must

be constant. The reduced form of the chemical potential of the subregion located at **r** then takes on the form,

$$\frac{\mu}{k_{\mathrm{B}}\mathrm{T}} = \Psi_M(\mathbf{r}) + \frac{\mu_{\mathrm{ions}}(\mathbf{r})}{k_B T}, \tag{1}$$

where the reduced potential due to all the colloidal particles is given by the sum

$$\Psi_M(\mathbf{r}) = \lambda_B \sum_{m=1}^{M} \frac{Z_m}{a_m |\mathbf{r}_m|}. \tag{2}$$

$|\mathbf{r}_m| = |\mathbf{R}_m|/a_m$ is the reduced distance from the center of the mth macroion of radius a_m and charge Z_m, and the chemical potential due to the microions in the region is

$$\mu_{\mathrm{ions}}(\mathbf{r}) = \sum_{j=1}^{J_s} \mu_j(\mathbf{r}) = \sum_{j=1}^{J_s} \{\mu_J^o + k_B T \ln[\gamma_j(\mathbf{r}) C_j(\mathbf{r})]\}, \tag{3}$$

where J_s is the number of ion types, $C_j(\mathbf{r})$ is the molar concentration of the jth ion type, and $\gamma_j(\mathbf{r})$ is the activity coefficient that reflects the electrical interactions of the microion. The microion concentration at any arbitrary position in the medium is therefore determined by the value of the cumulative potentials of all the macroions in the system, $\Psi_M(\mathbf{r})$, as given by Eq. (2). It is noted that to a first approximation $\Psi_M(\mathbf{r})$ is assumed to dominate the microion-microion pairwise interactions as the charge on the macroion is two or more orders of magnitude larger than that of the microions. Hence counterion-counterion correlations are expected to be significant primarily in regions near the surface of the macroion where the counterion concentrations are the largest. If this is the case then the force due to the macroions acting on the microions is given by the negative gradient $-\nabla\Psi_M(\mathbf{r})$. Hence the function $\nabla\Psi_M(\mathbf{r})$ serves in a similar manner in colloidal systems as the function $\nabla\rho_e$ is the molecular systems since both functions reflect the disposition of the more mobile charged species.

III. BROWNIAN DYNAMICS SIMULATIONS

Since the vector gradient $\nabla\Psi_M(\mathbf{r})$ determines the force exerted on the microions for a fixed array of macroions, the natural choice is to employ Brownian dynamics (BD) simulation methods to determine the disposition of the microions in the system. In this regard the macroions are in a fixed location and the microions are moved by a two-step process: first, by the total force acting on each microion due to all of the charged particles in the system, and second, by a superimposed ''random force'' to mimic the action of the solvent on the microions.

A. The mechanics

The BD evolution in time of the jth microion is given formally by the expression

$$q_j^{k+1} = q_j^k + \beta D_j \Delta t F_j + \omega\sqrt{D_j \Delta t}, \tag{4}$$

where D_j is the diffusion coefficient, Δt is the time interval for the move after k previous such moves, $-1 \leqslant \omega \leqslant +1$ is a random number, and F_j is the electrical force exerted on the jth microion by all of the other particles present,

$$F_j = -Z_j q_e \nabla_j \Psi_M - Z_j q_e \sum_{i \neq j} \nabla_j \varphi_i, \tag{5}$$

where Z_j is the charge of the jth microion, q_e is the magnitude of the electron charge, and φ_i is the reduced potential for the ith microion. The gradients are taken with respect to the relative distances between the participating particles. In all cases the unscreened Coulomb potential was employed.

The BD simulations follow standard methods [21]. In practice the following substitution is made for the simulations, $2D\Delta t = \langle S^2 \rangle$, where S is a stepsize whose value is proportional to the radius a_c of the counterion, viz., $S = M a_c$, where M is a multiplicative factor. All of the distances employed in these calculations were scaled to the radius of the macroion. The step size in the simulations was thus $s^r = S/a_p$. We performed calculations in which all of the parameters are scaled to the radius of the macroions, leading to the reduced parameters used in these simulations: $a_p^r = 1$ and $a_c^r = a_c/a_p$.

A rectangular box was used with the relative dimensions (in units of the macroion radius) reflective of the volume fraction of the system, which in all cases was $\phi_p = 0.01$. The longest dimension was taken to be along the Z axis. Hence the rectangular dimensions in reduced numbers were calculated from the relationship

$$r_X r_Y r_Z = r_X^2 r_Z = \left(\frac{N_p}{\phi_p}\right), \tag{6}$$

where N_p is the total number of colloidal particles. The reduced dimensions r_X and r_Z were chosen such that for the uniform distribution configuration the distance of the extreme macroions to the cell walls was the same in all directions.

Following Stevens, Falk, and Robbins [22] the macroions are at fixed locations and the microions are moved in accordance with Eqs. (4) and (5). For all simulations the macroions had the charge $Z_p = 50$ and the radius $a_p = 100$ Å, and the microions were of unit charge and radius $a_m = 1$ Å. Two cluster configurations were considered, a diamond shape and a simple cubic shape. A diamond-shaped cluster composed of seven particles, one at the center of the cluster and the other six along the positive and negative coordinates at reduced ''local'' coordinates d. The eight particles in the simple cubic lattice were also with reduced local coordinates $+/-d$. The centers of the two clusters in these simulations were at the reduced distance $2D_Z$ along the Z axis of the rectangle.

The BD simulations of the microions are performed in two stages: a preliminary calculation to ''equilibrate'' the system, usually consisting of 10^6 iterations for each microion in the system; and a ''final'' calculation of 10^6 iterations. Hard-sphere overlap with other particles, i.e. interpenetrating, was checked after each move, and the particle was returned to its initial position if the test was positive.

All calculations were performed on the DEC Alpha AXP2100/M500 at the University of Missouri Computing Facilities. The results were then expressed in graphics form using MATHEMATICA®

B. Estimates of the thermodynamic function

The partition function for the system Q was calculated from the accepted moves for all of the microions in the system for a particular configuration J, and summed over all configurations J,

$$Q=\sum_{J}\ \exp(-\beta E_J), \tag{7}$$

the reduced average internal energy $\beta\langle E_{\rm sys}\rangle$ was calculated from standard expression in statistical mechanics,

$$\beta\langle E_{\rm sys}\rangle=\beta\frac{\sum_{J}\ E_J\exp(-\beta \mathrm{E_J})}{\mathrm{Q}}, \tag{8}$$

and the reduced Helmholtz free energy $\beta\langle A_{\rm sys}\rangle$ from

$$\beta\langle A_{\rm sys}\rangle=-\ln(\mathrm{Q}). \tag{9}$$

C. Determinations of the microion distributions

Three different methods were used to characterize the disposition of the microions in the systems under study. The *projection distribution function* $N(z)$ is based on the symmetry of the computation cell. The basis of this distribution function is the radial distribution function for spherical symmetric cases, where the three-dimensional Cartesian coordinates are collapsed to the one-dimensional radial distribution. In the present case the projection is onto the Z axis, which is defined as the long axis of the rectangular computation cell. The second type of distribution function is the *real space distribution function* $S(x,y,z)$, where the entire computation cell is subdivided into identical boxes in all three directions. The set of numbers $\{S(x,y,z)\}$ were the accumulated values of the occupancy number of particles overall of the computation cycles $N_{\rm cycle}$. Clearly the determination of $N(z)$ is much less time intensive and memory intensive than $S(x,y,z)$. The third representation of the counterion distribution is through the constant concentration contours. These contours were determined from the same data set as employed for $S(x,y,z)$.

1. Projection distribution function

The number distribution of microions along the Z axis, $N(z)$, was determined by "slicing" the Z axis into 500 equally spaced volumes, or bins. The volume of each bin was thus

$$V_s=F_X^2 r_Z(500)=r_X^2\Delta r_Z, \tag{10}$$

where Δr_Z is the "thickness" of the bin. A microion is said to be in "bin number b" if its Z coordinate lies in the range $(b-1)\Delta r_Z$ to $b\Delta r_Z$ from the $-r_Z/2$ face of the rectangular box. The number average $N(z)$ was then determined by the total number of microions found in bin "b" divided by the total number of iteration cycles $N_{\rm cycl}$ in the simulation. The projection distribution functions $N(z)$ were determined separately for the counterion species and the coion species.

2. Real space distribution function

We determined the real space distribution function $S(x,y,z)$ to assess the redistribution of the microions with the change in the relative positions of the macroions. For this exercise we chose three cubic array clusters.

The rectangular computation box was subdivided into "bins" of 50 in number along the Z axis and 24 in number along both the X and Y axes, resulting in a total number of 28 800 identical subcells of dimensions in reduced lengths $\Delta r_X\Delta r_Y\Delta r_Z$. A microion is said to be in a certain subcell (a,b,c) if its reduced coordinates x, y, and z lie within the ranges $(a-1)\Delta r_X$ to $a\Delta r_X$, $(b-1)\Delta r_Y$ to $b\Delta r_Y$, and $(c-1)\Delta\ \Delta r_Z$ to $c\Delta r_Z$, respectively. The number $S(x,y,z)$ was then determined by the total number of microions found in the subcell as accumulated over the number of cycles $N_{\rm cycl}$ in the simulation. The real space distribution functions $S(x,y,z)$ were determined separately for the counterion species and the coion species.

The graphic representation of a three-dimensional real space distribution presents three major problems in regard to a quantitative presentation of the results. First, there is a much larger number of the counterion species than the coions due to the large charge of the macroions in these simulations. The second problem is that the counterions congregate in the vicinity of the macroions. Thus a common linear scaling of both the counterion and coion distributions will be sensitive only to the counterions near the macroions. The third problem is that any space-filling attempts to represent the three-dimensional microion densities in a two-dimensional space will show only the foremost (to the viewer) subcell populations. We therefore chose the following method to represent the BD simulation results. To overcome the first problem we simply chose not to compare directly the numbers of counterions with the coions. The counterions and coions are treated as two independent sets, and each set normalized to the largest subcell occupation number $S_{\rm max}$. The relative populations in each set thus lie in the range $1\geqslant S_j/S_{\rm max}\geqslant 0$. The third problem was overcome in two ways. First, graphic representation of the relative population of each set $\{S/S_{\rm max}\}$ was given by the linear scaling of both the radius and the shading of the point representing each of the 28 800 subcells, where the larger the radius and the darker the shading indicated the larger number population. The size of the representative point $p_{\rm size}$ thus varied over the range $\Delta x\geqslant p_{\rm size}\geqslant 0$ and the shading over the range $0.7\geqslant$ shade $\geqslant 0$, where "0" is "black" and "1" is "white." Using this duplicity in representation one can display the entire three-dimensional graphics for the counterion species since, as previously mentioned, they congregate in the vicinity of the macroions. In the case of the coions advantage was taken of the symmetry of the computation cell. In this case only half of the cell in the X direction is required and therefore the interior structure of the cluster can be open to examination. Because the coions tend to avoid the macroions,

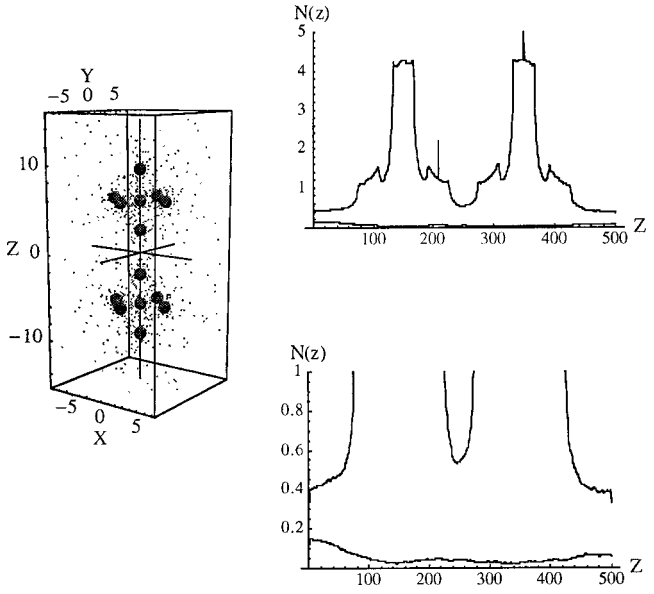

FIG. 1. $N(z)$ as a function of the bin number for the reference structure of a diamond configuration with maximum separations. The 14 colloidal particles have charge $Z_p=50$ and radius $a_p=100$ Å. The microions consist of 700 counterions and 25 added salt particles giving a total of 750 microions. The characteristic parameters of the cluster configuration are $d=+/-3.5$ along each local axis with a center-to-center separation distance $2D_Z=13$. The relative dimensions of the rectangular box are $r_X=r_Y=15$ and $r_Z=30$ for the volume fraction $\phi_p=0.01$. The amplitude factor is $M=3$. The average reduced energies of the above configuration are $\beta\langle E_{\mathrm{sys}}\rangle=-2.347\times10^6$ from Eq. (8) and $\beta\langle A_{\mathrm{sys}}\rangle=-5401$ from Eq. (9).

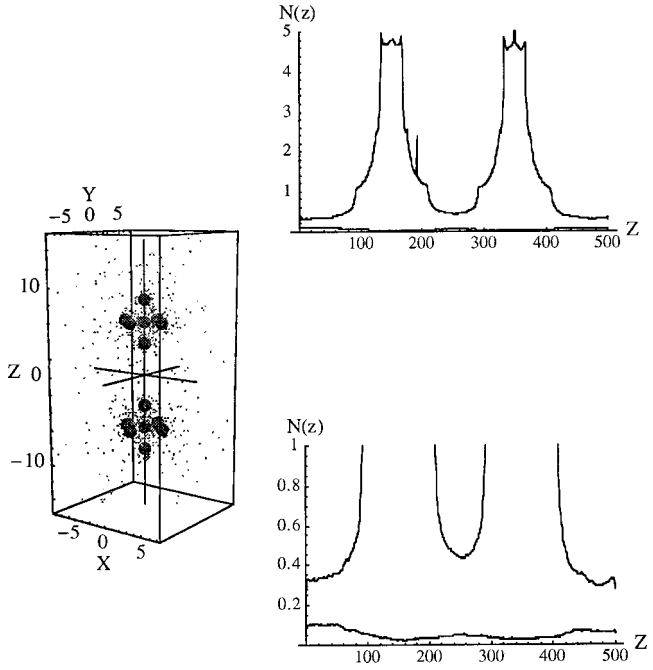

FIG. 2. $N(z)$ as a function of the bin number for the diamond configuration with contracted cluster separation. The 14 colloidal particles have charge $Z_p=50$ and radius $a_p=100$ Å. The microions consist of 700 counterions and 25 added salt particles giving a total of 750 microions. The characteristic parameters of the cluster configuration are $d=+/-2.5$ along each local axis with a center-to-center separation distance $2D_Z=11$. The relative dimensions of the rectangular box are $r_X=r_Y=15$ and $r_Z=30$ for the volume fraction $\phi_p=0.01$. The amplitude factor is $M=3$. The average reduced energies of the above configuration are $\beta\langle E_{\mathrm{sys}}\rangle=-2.058\times10^6$ from Eq. (8) and $\beta\langle A_{\mathrm{sys}}\rangle=-4237$ from Eq. (9).

the radius of the coions is greatly reduced in the center region thus exposing the more remote subcells. The second problem pertains only to the counterions, and is overcome by employing a ''clipping'' method. In these simulations all subcells with the value $S_j/S_{\max}>0.1$ is represented by a point size $p_{\mathrm{size}}=\Delta x$ and a shade of ''0.'' All other populations varied linearly with the ratio $S_j/S_{\max}$ over the ranges $\Delta x \geqslant p_{\mathrm{size}} \geqslant 0$ and $1 \geqslant \mathrm{shade} \geqslant 0$.

3. Contours of constant concentration

Constant ''relative'' concentration contour plots were obtained for each reduced set $\{S_j/S_{\max}\}$ by using the *ListContourPlot3D* package in MATHEMATICA®. Although several contours were examined, the contours $S_j/S_{\max}=0.043$ were chosen to compare the results for different separations in the cubic array. It is understood that these contours do not directly compare the relative concentrations in these sets because the distribution of the counterions differs for each system and therefore $S_{\max}$ must likewise vary in value and subcell location.

IV. BROWNIAN DYNAMICS SIMULATIONS—RESULTS

Shown in Fig. 1 is the diamond cluster configuration of maximum separation in these simulations and the number distributions $N(z)$ for the counterions and the coions in which 25 added salt particles (50 microions) are present. This reference system configuration employs the largest separation distance in this set of simulations with $d=3.5$ and a center-to-center separation distance of $2D_Z=13$ in relative separation units. The total system reduced interaction energy $\beta\langle E_{\mathrm{sys}}\rangle$ and Helmholtz free energy $\beta\langle A_{\mathrm{sys}}\rangle$ were calculated from Eqs. (8) and (9), respectively. Similar information is given in Fig. 2 in which the separation distances are $d=2.5$ and $2D_z=11$. Shown in Fig. 3 is the same information for the two cluster system in which $d=2.5$ with the two clusters now at a closer distance of $2D_Z=9$.

Attention is now directed to the simple cubic cluster system at the single cell level. The configuration shown in Fig. 4 represents a uniform distribution of the 16 colloidal particles in this system. The reduced local coordinate is $d=3.5$ and the center-to-center separation distance, if one were to associate this configuration with two identical clusters, is $2D_Z=14$. In Fig. 5 the value of d is 2.5 and the center-to-center separation distance is correspondingly increased to $2D_Z=15$. Shown in Fig. 6 is the configuration for $d=2.5$ but the two clusters are brought closer together for a center- to-center separation distance of $2D_Z=13$.

The spatial distribution functions $S(x,y,z)$ for the counterion species and the coions are shown in Fig. 7 for two simple cubic arrays, that on maximum separation (top) and

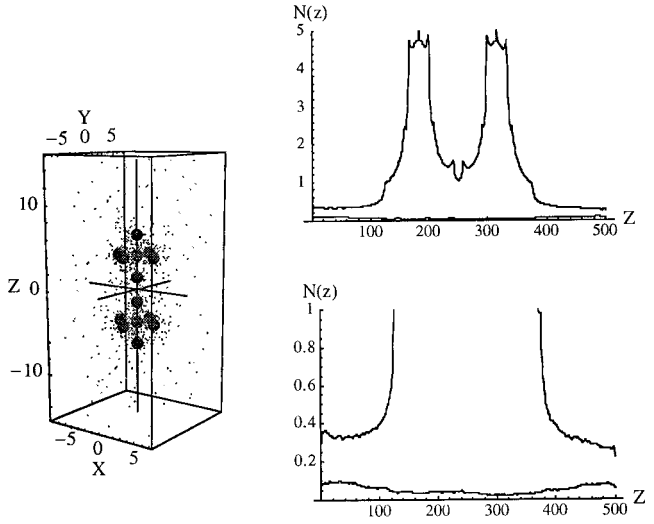

FIG. 3. $N(z)$ as a function of the bin number for the diamond configuration with minimum cluster separation. The 14 colloidal particles have charge $Z_p=50$ and radius $a_p=100$ Å. The microions consist of 700 counterions and 25 added salt particles giving a total of 750 microions. The characteristic parameters of the cluster configuration are $d=+/-2.5$ along each local axis with a center-to-center separation distance $2D_Z=9$. The relative dimensions of the rectangular box are $r_X=r_Y=15$ and $r_Z=30$ for the volume fraction $\phi_p=0.01$. The amplitude factor is $M=3$. The average reduced energies of the above configuration are $\beta\langle E_{\mathrm{sys}}\rangle=-1.408\times10^6$ from Eq. (8) and $\beta\langle A_{\mathrm{sys}}\rangle=-1054$ from Eq. (9).

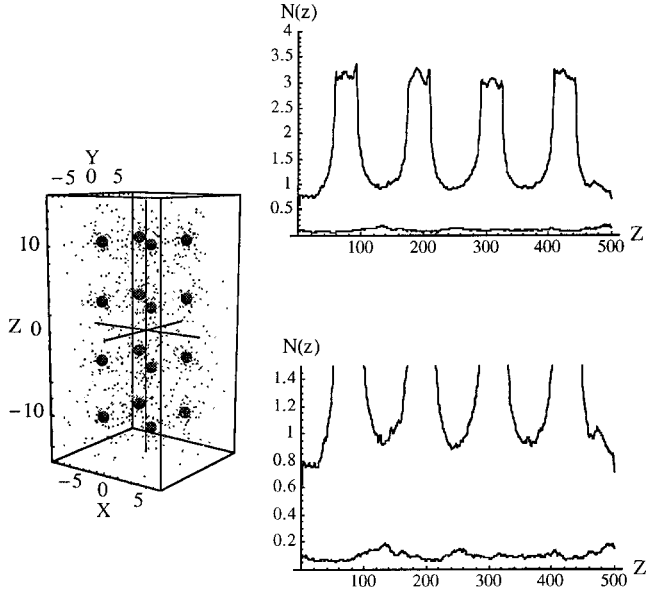

FIG. 4. $N(z)$ as a function of the bin number for the simple cubic configuration with maximum cluster separation. The 16 colloidal particles have charge $Z_p=50$ and radius $a_p=100$ Å. The microions consist of 800 counterions and 50 added salt particles giving a total of 900 microions. The characteristic parameters of the cluster configuration are a cubic cell for a local reduced distance $d=3.5$ and a center-to-center separation distance $2D_Z=14$. The relative dimensions of the rectangular box are $r_X=r_Y=15$ and $r_Z=30$ for the volume fraction $\phi_p=0.01$. The amplitude factor is $M=10$. The average reduced energies of the above configuration are $\beta\langle E_{\mathrm{sys}}\rangle=-9.043\times10^5$ from Eq. (8) and $\beta\langle A_{\mathrm{sys}}\rangle=-1030$ from Eq. (9).

minimum separation (bottom). Because the counterions tend to accumulate in the vicinity of the macroions, the distribution $S(x,y,z)$ shown at the top left of this figure is representative of other macroion distributions. This is because the elements of the unclipped representation of $S(x,y,z)$ are dominated by the counterions in the vicinity of the macroions and all detail is lost for their distribution in the majority of the volume of the system. Most of the computation cell appears ''empty'' as a result. Shown at the top left is the corresponding coion distribution $S(x,y,z)$. In contrast the coions are more or less uniformly distributed throughout the computation cell except in the vicinity of the macroions, where their presence is excluded due to the large macroion-coion repulsive interaction. To show the contrast in the distribution of the coions only a portion of the computation cell can be displayed. Both coion figures are centered on the location of the macroions along the X axis. The bottom figure represents a ''head on'' view of $S(x,y,z)$ for the case of minimum separation distance of the macroions. Clearly the coions are of lesser concentration in the interior of this cluster than for the case of maximum macroion separation simulations summarized in the top left of the figure.

We examine in more detail the distribution of the counterions and the coions for the maximum and minimum separation distances in Figs. 8 and 9. At the top of Fig. 8 is the top view of the slice in the range $4.0>Z>3.0$ of the computation cell for the *clipped function* $S(x,y,z)$ of the maximum separation distance cluster. The bottom figures are for the same slice except more focused on the interior of the macroion array. The lower left figure is the clipped $S(x,y,z)$ function for the counterions and the lower right for the coions. These simulations indicate that the coions avoid the macroions but are of significant concentration in the interior of the cluster. A similar set of graphics is given in Fig. 9 for the system of minimum macroion separation. Note that as the macroions are drawn closer together in the array the counterion concentration tends to increase in the interior of the cluster whereas the coions are more excluded.

Constant concentration contour plots were determined for the reduced spatial concentration distributions $S(x,y,z)/S_{\max}$. The constant contour $S(x,y,z)/S_{\max}=0.043=C(x,y,z)$ was chosen to illustrate the influence of the macroion separation distance on the counterion distributions. Shown in Fig. 10 are three views of the contour plots for the system described in the caption of Fig. 4. The angle view of the top figure establishes the relative position of the macroions and the $C(x,y,z)=0.043$ surfaces. The lower left figure is the view in the Y-Z plane and the lower right figure is the X-Z plane view. The $C(x,y,z)=0.043$ contours apparently partition the macroions into ''pairs'' for the reduced local parameters $d=3.5$ and separation distance $2D_Z=14$.

Shown in Fig. 11 are two planar views of the contour plots $C(x,y,z)=0.043$ for the system described in the caption of Fig. 5. The left figure is the view in the Y-Z plane and the right is the X-Z plane. Absence of the macroions indicates that the $C(x,y,z)=0.043$ contours now engulf all of

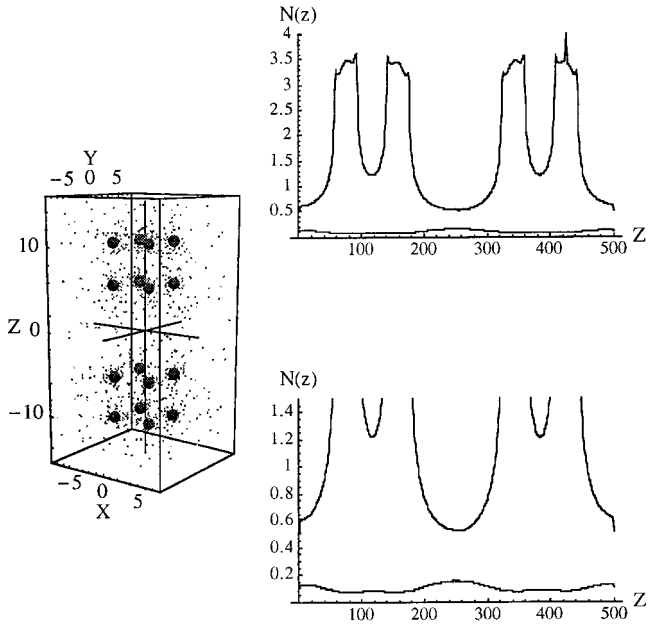

FIG. 5. $N(z)$ as a function of the bin number of the simple cubic configuration with contracted cluster separation. The 16 colloidal particles have charge $Z_p=50$ and radius $a_p=100$ Å. The microions consist of 800 counterions and 50 added salt particles giving a total of 900 microions. The characteristic parameters of the cluster configuration are a cubic cell with $d=2.5$ and a center-to-center separation distance $2D_Z=16$. The relative dimensions of the rectangular box are $r_X=r_Y=15$ and $r_Z=30$ for the volume fraction $\phi_p=0.01$. The amplitude factor is $M=10$. The average reduced energies of the above configuration are $\beta\langle E_{\rm sys}\rangle=-1.168\times10^6$ from Eq. (8) and $\beta\langle A_{\rm sys}\rangle=-1239$ from Eq. (9).

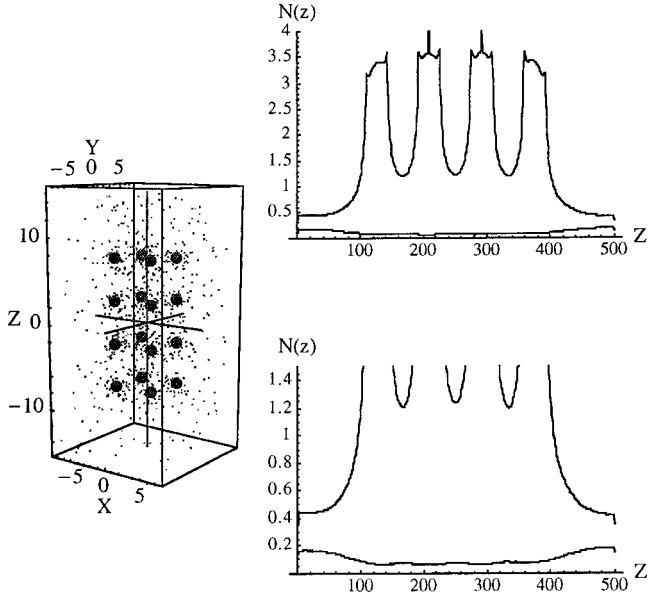

FIG. 6. $N(z)$ as a function of the bin number for the simple cubic configuration with minimum cluster separation. The 16 colloidal particles have charge $Z_p=50$ and radius $a_p=100$ Å. The microions consist of 800 counterions and 50 added salt particles giving a total of 900 microions. The characteristic parameters of the cluster configuration are a cubic cell with $d=2.5$ and a center-to-center separation distance $2D_Z=10$. The relative dimensions of the rectangular box are $r_X=r_Y=15$ and $r_Z=30$ for the volume fraction $\phi_p=0.01$. The amplitude factor is $M=10$. The average reduced energies of the above configuration are $\beta\langle E_{\rm sys}\rangle=-1.404\times10^6$ from Eq. (8) and $\beta\langle A_{\rm sys}\rangle=-2245$ from Eq. (9).

the macroions. The contour $C(x,y,z)=0.043$ partitions the system into two groups of eight macroions for $d=2.5$ and $2D_Z=16$. We now move these two cubic structures closer together, going from $2D_Z=16$ to $2D_Z=10$ while maintaining the value of $d=2.5$. The constant contour surfaces in the Y-Z and X-Z planes for this new situation are shown in Fig. 12. The relative concentration contours of $C(x,y,z)=0.043$ now encompass all of the macroions in the system.

V. DISCUSSION

In the past the stability of colloidal systems and the structural arrangements of the macroions were determined solely from macroion-macroion pair interaction energy, usually given as the DLVO form that is assumed to reflect the Helmholtz free energy change as two colloidal particles approach each other. The DLVO potential may be used to interpret structural transitions in the system [23]. For example, the body-centered-cubic (bcc) to face-centered-cubic (fcc) transition upon increasing the colloid concentration [24] may be viewed as a packing problem with the purely repulsive pairwise interaction leading to a reduction in the electrostatic stress on the system. The long range repulsion of the DLVO potential results in a crystalline structure that extends throughout the medium. Such long range repulsion does not lend itself to heterogeneous structures observed by DVM methods [1–4].

One tenet of the DLVO model is that the structure of the ion cloud about the isolated colloidal particle is only slightly perturbed by the presence of a second colloidal particle. This concept is clearly illustrated in Fig. 3 in the paper by Warren [13], and should hold ''true'' as long as the colloidal particles are not too close to each other. The usual ''yardstick'' to measure the ''thickness'' of the ion cloud about a colloidal particle is the reciprocal of the screening length, $1/\kappa$. As long as the distance between any two colloidal particles is greater than $1/\kappa$ one may describe the properties of a colloidal system solely on the basis of a ''pair interaction.'' Okubo has even proposed that the physical properties of dilute colloidal suspensions can be interpreted in terms of an ''effective hard sphere radius'' equal to $1/\kappa$ [25,26].

A conceptual problem arises, however, if the separation distance between two colloidal particles is less than $1/\kappa$, where the ion clouds of the two macroions have extensive overlap. For example, the situation may obtain in which the counterions originally assigned to colloidal particle ''*A*'' may in fact be much closer to colloidal particle ''*B*.'' One cannot therefore ignore the interactions of the counterions with colloidal particles other than their parent. This is one of the criticisms of Langmuir [27] in 1938 regarding the pair interaction energy approach. As also pointed out by Langmuir this energy approach did not allow for the entropic contributions of the microions to the free energy of the system. Langmuir proposed an alternative theory in which the counterions were treated on a more or less equal footing as the macro-

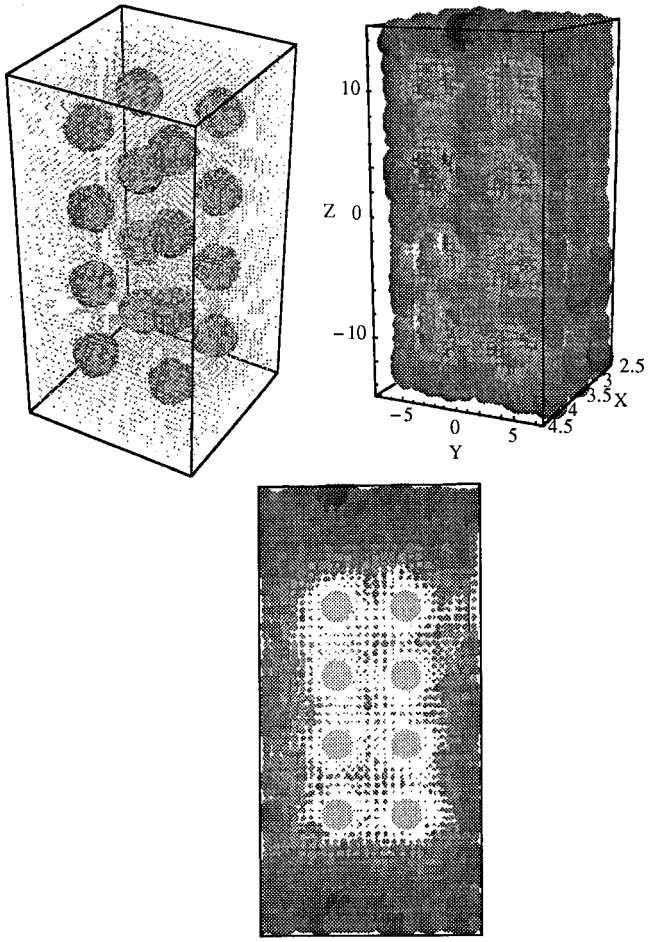

FIG. 7. Concentration density $S(x,y,z)$ for simple cubic configuration. The system is that described in the caption of Fig. 4. Shown on the top left is $S(x,y,z)$ for the counterions for the entire computation cell volume for the system described in Fig. 4. Shown on the top right is $S(x,y,z)$ for the coions in a volume slice $4.5>X>2.5$, which is centered on the macroion location. The figure at the bottom is the coion distribution for the system described in Fig. 6, where the macroion separation is minimal. Note that in this case the coions are virtually excluded from the interior of the cluster. These density maps indicate that the counterions are localized in the vicinity of the individual macroions and that the coions are excluded from the region near the macroions but may permeate throughout the colloidal structure.

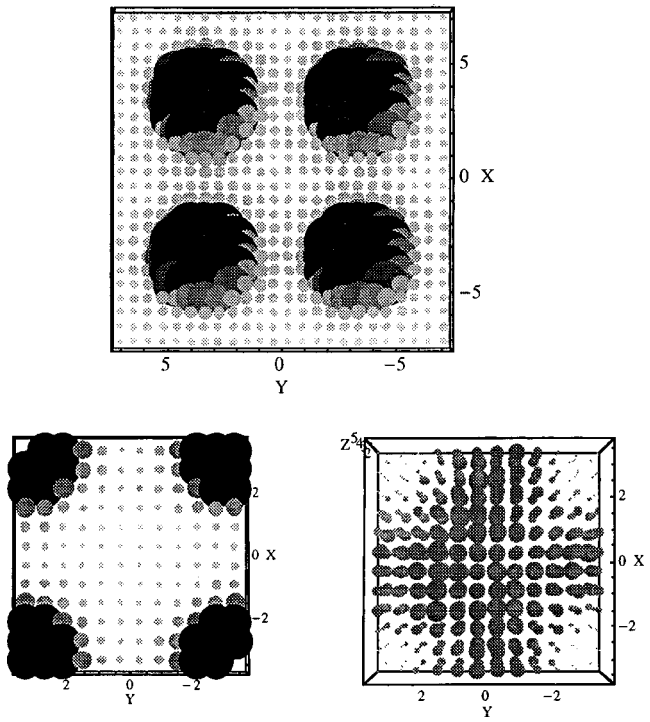

FIG. 8. Clipped concentration density $S(x,y,z)$ for the interior of the simple cubic configuration with maximum cluster separation. The system is that described in the caption of Fig. 4. The values of $S_{\max}$ for the counterions and coions are, respectively, 968 700 and 4826. The cutoff value of $S/S_{\max}=0.1$ was used for the counterions. The top figure is the counterion distribution in the volume of a "slice" of the computation cell for which $4.5>Z>2.5$. The bottom left figure is $S(x,y,z)$ for the counterions within the interior of the cubic array bounded by $-3.5>X>3.5$, $-3.5>Y>3.5$, and $4.5>Z>2.5$. The counterions accumulate near the surface of the macroions. The bottom left figure is $S(x,y,z)$ for the coions within the interior of the cubic array bounded by $-3.5>X>3.5$, $-3.5>Y>3.5$, and $4.5>Z>2.5$. The coions are excluded near the surface of the macroion and their concentration is a relatively larger interior to the cluster with an apparent "maximum" in the center of the cluster.

ions. The distribution of the counterions exhibited a *structure* in the solution, playing the role of alternating negative charge to the positive macroion charge. Inclusion of the counterions resulted in a system in which the total energy was negative as in the case of true crystalline structures such as sodium chloride. Verwey and Overbeek [9] argued against the model of Langmuir [27] and since that time the DLVO potential has been the premier paradigm for the interpretation of data on colloidal systems. The role of the microions was relegated to a passive role acting solely through the screening parameter.

The VT theories have resurrected the importance of the microion contribution to the stability of the structures of colloidal systems. Unlike the Langmuir model the microions need not be structured in the solution but rather be of two different concentrations in the two phase regions such as to maintain both the constant chemical potential and electrical neutrality of each phase. As a consequence the total energy of the system was again found to be *negative*.

It was previously suggested that the stability of a macroion system [18–20] might be treated in a manner analogous to that of a conjugated chemical system proposed by Bader [16,17]. In these papers the potential field set up solely by the macroions was considered to reflect the distribution of the counterions. With this formalism one might be able to identify "stable clusters" as those structures capable of supporting extensive sharing of the counterions as a conjugated chemical system is stabilized by the dislocation of the electrons in the bonding scheme. The present study examines directly the counterion and coion distributions by means of computer simulations using BD expressions for the movement of the microions.

The initial analysis of the BD results in the rectangular simulation cell is analogous to that for spherical symmetry,

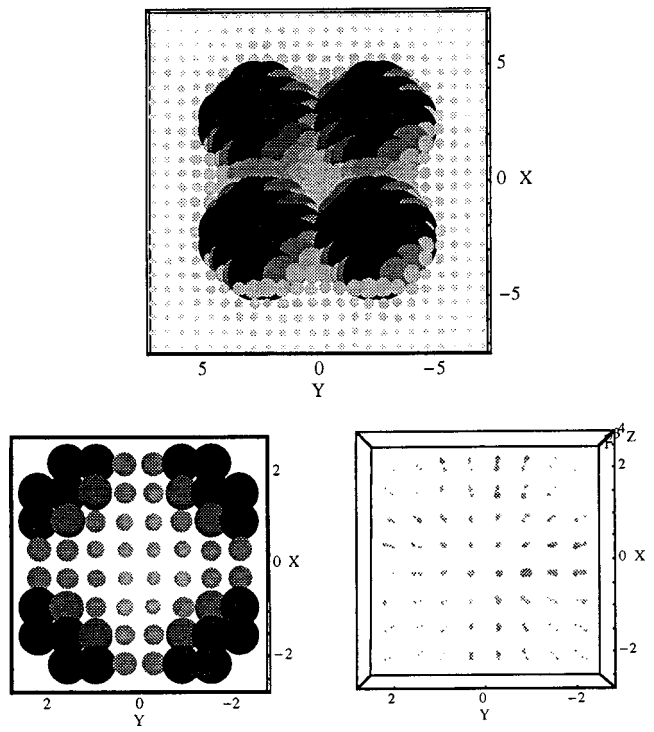

FIG. 9. Clipped concentration density $S(x,y,z)$ for the interior of the simple cubic configuration with the minimum cluster separation. The system is that described in the caption of Fig. 6. The values of $S_{\max}$ for the counterions and coions are, respectively, 998 900 and 4982. The cutoff value of $S/S_{\max}=0.1$ was used for the counterions. The top figure is the counterion distribution in the volume of a ''slice'' of the computation cell for which $3.5>Z>1.5$. The bottom left figure is $S(x,y,z)$ for the counterions within the interior of the cubic array bounded by $-2.5>X>2.5$, $-2.5>Y>2.5$, and $3.5>Z>1.5$. The counterions accumulate near the surface of the macroions with an increase in density in the interior of the array. The bottom left figure is $S(x,y,z)$ for the coions within the interior of the cubic array bounded by $-2.5>X>2.5$, $-2.5>Y>2.5$, and $3.5>Z>1.5$. In comparison with Fig. 8 the lighter shading and smaller point size indicates more coions are excluded from the interior of the cluster.

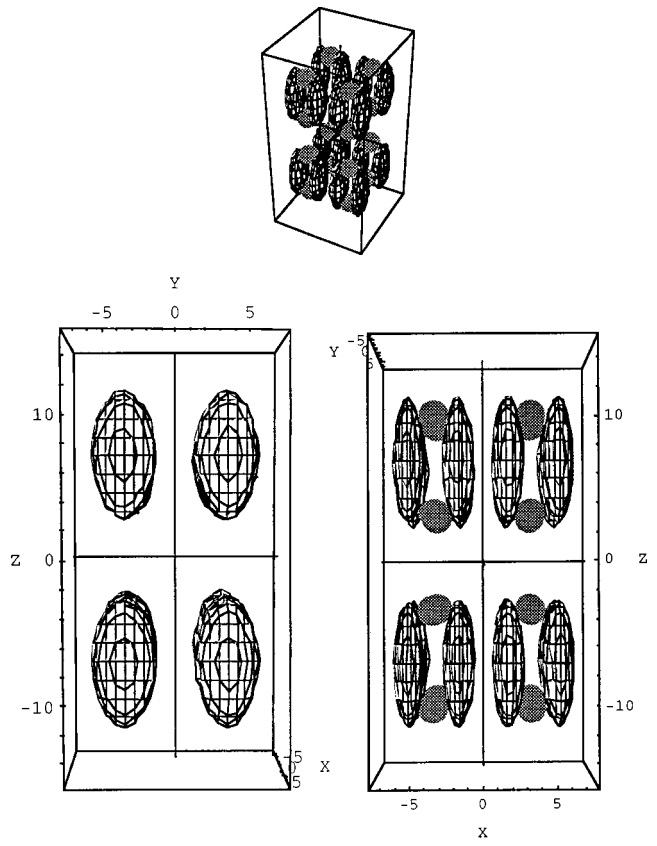

FIG. 10. Concentration contours for a cubic array with $d=3.5$ and $2D_Z=14$. The system is that described in the caption for Fig. 4, where $d=3.5$ and $2D_Z=14$. The constant concentration contour is $C(x,y,z)=S/S_{\max}=0.043$. The top figure is an angle view of the computation cell, where the macroion locations are indicated by the solid points. The lower left figure is the view in the Y-Z plane and the lower right in the X-Z plane.

where the angular dependence is projected onto a radial plot. In the present case the projections are along the Z axis. In the determination of the number distributions $N(z)$ no correction was made for the finite size of the macroions which clearly excludes microions by construct of the simulation. Consider the volume of the ''slice'' given by Eq. (10). The maximum volume that the colloidal particles can occupy in this slice depends upon the girth of the macroion and the number of macroions. Since by construction at most only four macroions can invade any one slice of the $N(z)$ determination. Thus the volume of the macroions at maximum girth in reduced coordinates is $V_{sp}=4\pi\Delta r_Z$ since the reduced radius is unity. Therefore the *maximum* contamination of the macroions is reflected in the ratio $V_{s,p}/V_s=4\pi/r_X^2$, or approximately 0.06 for the dimension $r_X=15$. This small correction factor is not sufficiently significant to affect the discussions on the distributions $N(z)$.

Attention is first given to Figs. 1–3 for the diamond clusters. While there appears to be some form of symmetry in $N(z)$ about the central macroion of each cluster, there is a noticeable asymmetry about the exterior macroions. It is quite clear that the counterions are largely drawn to the interior of the cluster and virtually centered about the central macroion of each cluster. As the distance between the macroions within the cluster contract the details of the outer macroion locations tend to become more obscure as the counterion distributions begin to strongly overlap, a conclusion drawn in comparison to Figs. 1 and 2. As deduced from Figs. 2 and 3, when clusters of fixed dimensions are brought closer together the counterions tend to migrate to the region between the clusters. The functions $N(z)$ for the coions indicate that they populate regions between the clusters if the clusters are sufficiently far apart, as indicated by the ''maximum'' in the central bins, but decreases slightly as the clusters are brought together.

The simulations of the cubic clusters in Figs. 4–6 show similar behavior in the $N(z)$ distribution functions. In the ''uniform'' macroion distribution shown in Fig. 4 the coions are more or less uniformly distributed with a slightly higher

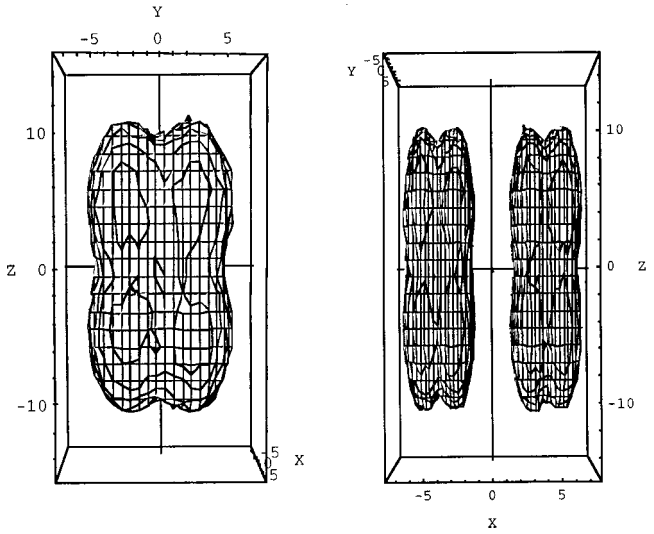

FIG. 11. Concentration contours for cubic array with $d=2.5$ and $2D_Z=16$. The system is that described in the caption for Fig. 5, where $d=2.5$ and $2D_Z=16$. The constant concentration contour is $C(x,y,z)=S/S_{\max}=0.043$. The left figure is the view in the Y-Z plane and the right view is in the X-Z plane.

concentration between the macroions. When the value of d is contracted from 3.5 to 2.5 the distance between the two clusters increases by a corresponding amount. A comparison of Figs. 4 and 5 indicates that the coions now increase their occupancy in the region between the clusters with a concomitant exclusion from the interior of each cluster. Upon movement of these clusters to a separation distance that results in ''one cluster,'' viz., Fig. 6, the coions are further excluded from the interior of the array.

A more detailed analysis of the three-dimensional distribution of the counterion species and the coions is effected through the spatial function $S(x,y,z)$. The uniform distribution case ($d=3.5$ and $2D_Z=14$) is shown in the top two graphics in Fig. 7. The counterions mainly reside in the vicinity of the macroions and the coions are virtually distributed in a uniform manner throughout the computation cell, with a slightly depressed concentration in the vicinity of the macroions. This distribution of counterions and coions is also evident in Fig. 4. In contrast the bottom graphic of Fig. 7 for the $d=2.5$ and $2D_Z=10$ system clearly shows the exclusion of the coions from the interior of the cluster with the build up exterior to the cluster. These behaviors are also reflected in $N(z)$ in Fig. 6. Turning now to the slice interior to the cluster shown in Fig. 8 for $d=3.5$ and $2D_Z=14$, we find that the coions appear to congregate in the center of the structure. This central congregation results in the appearance of the more or less uniform distribution of coions shown in the projection plot of Fig. 4. We now contrast these results with those for the most compacted structure for $d=2.5$ and $2D_Z=10$ as given in Fig. 9. In this case the counterions are drawn into the interior of the cluster and the coions are virtually excluded. These distributions are also evident in the projection profiles shown in Fig. 6.

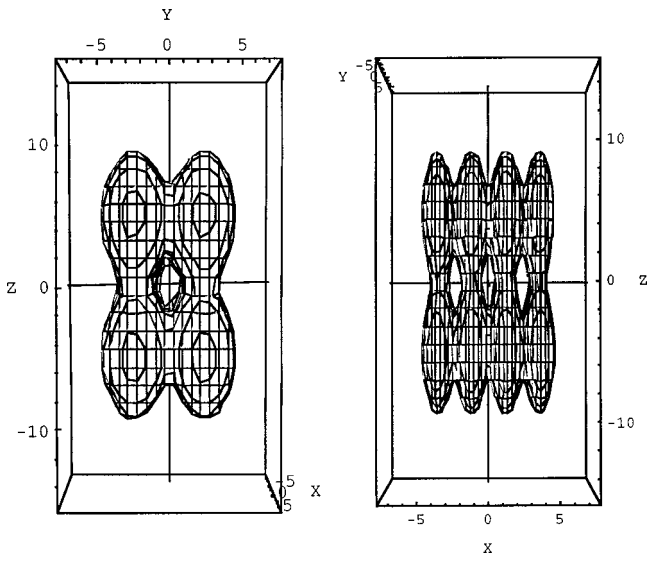

FIG. 12. Concentration contours for cubic array with $d=2.5$ and $2D_Z=10$. The system is that described in the caption for Fig. 5, where $d=2.5$ and $2D_Z=10$. The constant concentration contour is $C(x,y,z)=S/S_{\max}=0.043$. The left figure is the view in the Y-Z plane and the right view is in the X-Z plane.

Attention is now given to the counterion concentration contours $C(x,y,z)=0.043$ shown in Figs. 10–12 for the three cubic systems. These contours result not only from the potential field set up by the stationary macroions, viz., the JPF paradigm, but also from the interactions with the other microions in the system in accordance with Eqs. (1)–(3). The choice of $C(x,y,z)=0.043$ is somewhat arbitrary but chosen by trial and error to illustrate the correlations between macroions. Obviously a value of $C(x,y,z)=0.005$ would not be instructive since these contours would envelop all of the macroions under the three conditions examined. Likewise a value of $C(x,y,z)>0.8$ would provide little insight as this would reflect counterions ''localized'' to the vicinity of their parent macroions as inferred from the profiles in Figs. 1–3. It is further emphasized that these contours are relative to the maximum counterion occupancy number in the 28 800 subcells. Hence both the location and the magnitude of $S_{\max}$ may vary for these three systems. It is for these reasons that conclusions drawn from a direct comparison of the contours in Figs. 10–12 may be viewed as suspect. However, one can make qualitative assessments regarding the physical situations arising from the variation of d and $2D_Z$ since the values of $S_{\max}$ vary only by a few percent. For example, $S_{\max}=968\,700$ for $d=3.5$ and $2D_Z=14$ whereas $S_{\max}=998\,900$ for $d=2.5$ and $2D_Z=10$. With these considerations in mind, we now interpret the contours in Figs. 10–12.

In the situation for which $d=3.5$ and $2D_Z=14$, the contours in Fig. 10 indicate that the macroions in the cubic cluster are partitioned in pairs aligned along the Z axis of the computation cell. These pairs are localized to their respective cubic cells. If one now changes the parameter d from 3.5 to 2.5 while increasing the distance $2D_Z$ from 14 to 16 the $C(x,y,z)=0.043$ contours extend to include the macroions of both cubic cells. Let us now draw the two cubic clusters in Fig. 11 closer to each other, with the resulting concentration contour shown in Fig. 12. It is evident that now the contour surface extends to all of the macroions in the system. If we

again draw upon the formalism of Bader, the configuration in Fig. 12 represents a highly conjugated system and should therefore be more stable than the structures in Figs. 10 or 11.

We address the reduced system interaction energy $\beta\langle E_{sys}\rangle$ and system Helmholtz free energy $\beta\langle A_{sys}\rangle$ for the ''diamond clusters'' and the ''simple cubic clusters.'' The reduced interaction energies for Figs. 1–3 are, respectively, $\beta\langle E_{sys}\rangle/10^6 = -2.347$, -2.058, and $=-1.408$, and the reduced Helmholtz free energies are, respectively, $\beta\langle A_{sys}\rangle = -5401$, -4237, and -1054. The corresponding values in the local parameter d are 3.5, 2.5, and 2.5 while the center-to-center distances are $2D_Z = 13$, 11, and 9. One may conclude that the approach of two diamond clusters leads to an unfavorable energy situation and therefore larger clusters may not form in this head-to-head manner. We now contrast this with the results for the cubic clusters. In going from $d=3.5$ to $2D_Z = 14$ and the values $d=2.5$ and $2D_Z=16$ the value of $\beta\langle E_{sys}\rangle/10^6$ changes from -0.9043 to -1.168 and $\beta\langle A_{sys}\rangle$ changes from -1030 to -1239. Within the context of the paradigm of the DLVO theory one might say that the increase in repulsion between the macroions in the same cluster is more than compensated for with the decrease in repulsion between the two microclusters as they become further separated. Let us now move the dual clusters of $d=2.5$ from $2D_Z=16$ to $2D_Z=10$. The energy values now change from $\beta\langle E_{sys}\rangle/10^6 = -1.168$ to -1.404 and $\beta\langle A_{sys}\rangle$ from -1239 to -2245. In other words the cluster configuration in Fig. 12 is more stable than the cluster configuration in Fig. 11.

We can account for the two different behaviors of the diamond and cubic clusters as follows. In the case of the diamond clusters, the head on approach does not permit the sharing of the counterions as a ''conjugated bonding system'' is not possible, or provide a meaning to the term ''exclusion of the coions.'' In contrast, the cubic system permits a ''sharing'' of the counterions along the Z axis as indicated, for example, in Figs. 10 and 11. As the two clusters approach each other a ''network'' system of counterion sharing is set up as shown by the contour surface in Fig. 12. In this configuration the ''conjugated'' system is extensive and the ''super cluster'' is stabilized. It is important to note that the coions are excluded from the interior of the ''super cluster'' as shown in Figs. 7 and 9. In this regard the VT theories provide an accurate partitioning of the coions into two regions, the macroion ''dense'' region having the lesser coion concentration [11,13]. However, concomitant with the coion exclusion are the influx of counterions into the interior of the cluster due to the cumulative contribution of the potential fields of the participating colloidal particles to any interior volume element. For those interior volume elements in the *vicinity of the macroion surfaces* the influx of counterions *reduces the value* of the ''effective charge'' of the macroion. Reduction in the effective charge was suggested on the basis of the JPF method [18] and recently verified by BD simulations where the effective charge was found to be dependent upon the lattice location of the macroion [28]. It is noted that Langmuir also suggested on thermodynamic arguments that the charge on the colloidal particles in the dense phase must be less that in the sparse phase [27]. Another consequence of the influx of counterions to the colloidal cluster is the formation of an extensive conjugated system for certain cluster geometries.

The orbital model of colloidal systems can also explain the presence of multiple clusters and the kinetics of growth of larger cluster domains from smaller cluster domains. The exclusion of the coions from the central core of the cluster results in a ''second double layer'' involving the coions as shown in Figs. 6 and 7. Such a second double layer was previously suggested on the basis of the JPF method [19].

The simulations performed in this study were based on the simple cubic lattice. It is of interest to note that Gröhn and Antonietti [29] reported a macroscopic phase separation of swollen microgels that was analyzed in terms of a simple cubic lattice.

VI. CONCLUSION

The BD simulations address the question as to what happens when the counterion clouds about the parent colloidal particles interpenetrate with other colloidal particles. The system responds to the electrical stress by forming dense and sparse regions of the macroions aided by the redistribution of the microions. In the dense regions the coions are excluded with an accompanying influx of counterions. The counterions in the dense region respond to the larger cumulative colloid contribution of the potential in the vicinity of the participating macroions by reducing the ''effective charge'' of the macroions in the cluster. Under certain geometries that promote ''conjugated bonding'' the increased mobility of the community-shared counterions tend to stabilize the cluster. As a consequence of the coion exclusion a ''second double layer'' is formed about the cluster which provides a kinetic barrier to cluster growth.

ACKNOWLEDGMENTS

I wish to acknowledge the Kyoto University Foundation for providing partial support during my visit with Professor Matsuoka in the Department of Polymer Chemistry of Kyoto University, and the many stimulating discussions with Professor Matsuoka and Dr. Gröhn regarding their research.

[1] N. Ise, T. Okubo, K. Ito, S. Dosho, and I. Sogami, Langmuir **1**, 176 (1985).

[2] K. Ito, H. Nakamura, H. Yoshida, and N. Ise, J. Am. Chem. Soc. **110**, 6955 (1988).

[3] A. E. Larsen and D. G. Grier, Nature (London) **385**, 230 (1997).

[4] M. D. Carbajal-Tinoco, F. Castro-Román, and J. L. Arauz-Lara, Phys. Rev. E **53**, 3745 (1996).

[5] N. Ise, H. Matsuoka, K. Ito, and H. Yoshida, Faraday Discuss. Chem. Soc. **90**, 13 (1990).

[6] K. Ito, H. Yoshida, and N. Ise, Chem. Lett. **1992**, 2081 (1992).
[7] K. Ito, H. Yoshida, and N. Ise, Science **263**, 66 (1994).
[8] H. Yoshida, N. Ise, and T. Hashimoto, J. Chem. Phys. **103**, 10146 (1995).
[9] E. J. Verwey and J. T. G. Overbeek, *Theory of the Stability of Lyophobic Colloids* (Elsevier, New York, 1948).
[10] I. Sogami and N. Ise, J. Chem. Phys. **81**, 6320 (1984).
[11] R. van Roij, M. Dijkstra, and J.-P. Hansen, Phys. Rev. E **59**, 2010 (1999).
[12] A. R. Denton, J. Phys.: Condens. Matter **11**, 10061 (1999).
[13] P. B. Warren, J. Chem. Phys. **112**, 4683 (2000).
[14] K. S. Schmitz and L. B. Bhuiyan, Phys. Rev. E **63**, 011503 (2000).
[15] K. S. Schmitz, Phys. Rev. E **65**, 061402 (2002).
[16] R. F. W. Bader, T. S. Slee, D. Cremer, and E. Kraka, J. Am. Chem. Soc. **105**, 5061 (1983).
[17] R. F. W. Bader, Acc. Chem. Res. **18**, 9 (1985).
[18] K. S. Schmitz, Langmuir **13**, 5849 (1997).
[19] K. S. Schmitz, Langmuir **15**, 4093 (1999).
[20] K. S. Schmitz, Phys. Chem. Chem. Phys. **1**, 2109 (1999).
[21] M. P. Allen and D. J. Tildesley, *Computer Simulations of Liquids* (Clarendon Press, Oxford Science Publications, Oxford, England, 1993).
[22] M. J. Stevens, M. L. Falk, and M. O. Robbins, J. Chem. Phys. **104**, 5209 (1996).
[23] R. Williams and R. S. Crandall, Phys. Lett. **48A**, 224 (1974).
[24] B. J. Ackerson, T. W. Taylor, and N. A. Clark, Phys. Rev. A **31**, 3183 (1985).
[25] T. Okubo, Acc. Chem. Res. **21**, 281 (1988).
[26] T. Okubo, Naturwissenschaften **79**, 317 (1992).
[27] I. Langmuir, J. Chem. Phys. **6**, 873 (1938).
[28] K. S. Schmitz, Langmuir **17**, 8028 (2001).
[29] F. Gröhn and M. Antonietti, Macromolecules **33**, 5938 (2000).